Article

Nanostructured AgPbSbTe System Bulk Materials with Enhanced Thermoelectric Performance

Min Zhou, Jing-Feng Li, and Takuji Kita

J. Am. Chem. Soc., **2008**, 130 (13), 4527-4532 • DOI: 10.1021/ja7110652

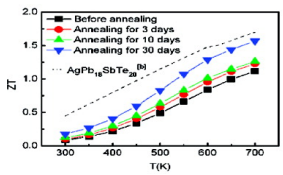

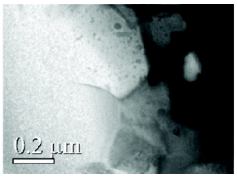

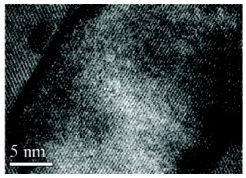

More About This Article

Additional resources and features associated with this article are available within the HTML version:

- Supporting Information
- Links to the 1 articles that cite this article, as of the time of this article download
- Access to high resolution figures
- Links to articles and content related to this article
- Copyright permission to reproduce figures and/or text from this article

View the Full Text HTML

J|A|C|S
ARTICLES
Published on Web 03/08/2008

Nanostructured $AgPb_mSbTe_{m+2}$ System Bulk Materials with Enhanced Thermoelectric Performance

Min Zhou,[†] Jing-Feng Li,*[,†] and Takuji Kita[‡]

State Key Laboratory of New Ceramics and Fine Processing, Department of Materials Science and Engineering, Tsinghua University, Beijing, 100084, China and Material Engineering Division III, Vehicle Engineering Group, Higashifuji Technical Center, Toyota Motor Corporation, 1200, Mishuku, Susono, Shizuoka, 410-1193, Japan

Received December 13, 2007; E-mail: jingfeng@mail.tsinghua.edu.cn

Abstract: Nanostructured $Ag_{0.8}Pb_{m+x}SbTe_{m+2}$ ($m = 18$, $x = 4.5$) system thermoelectric materials have been fabricated by combining mechanical alloying (MA) and spark plasma sintering (SPS) methods followed by annealing for several days to investigate the effect on microstructure and thermoelectric performance. It was found that appropriate annealing treatment could reduce both the electrical resistivity and the thermal conductivity at the same time, consequently greatly enhancing the thermoelectric performance. A low electrical resistivity of 2×10^{-3} Ohm-cm and low thermal conductivity of 0.89 W m^{-1} K^{-1} were obtained for the sample annealed for 30 days at 700 K. The very low thermal conductivity is supposed to be due to the nanoscopic Ag/Sb-rich regions embedded in the matrix. A high *ZT* value of 1.5 at 700 K has been achieved for the sample annealed for 30 days.

1. Introduction

Thermoelectric materials are becoming increasingly important in the field of energy harvesting and conversion. For a compound to be qualified as an efficient thermoelectric material it should exhibit a high thermoelectric figure of merit (Z) at the operating temperature (T). Z is defined as $Z = \alpha^2\sigma/\kappa$, where α, σ, and κ are the Seebeck coefficient, electrical conductivity, and thermal conductivity, respectively. Therefore, high-performance thermoelectric materials require a perfect combination of high power factor ($\alpha^2\sigma$) and low thermal conductivity κ. However, it is very difficult to control the above three parameters independently, which often counter each other, and all of them are restricted by the carrier concentration. The Seebeck coefficient is inversely related to the electrical conductivity according to the Boltzmann transport equation, and as a result, increasing electrical conductivity usually results in a decrease in the Seebeck coefficient. In addition, the reduction of thermal conductivity often leads to a decrease of electrical conductivity. Therefore, the main purposes of the research on thermoelectric materials are to increase electrical transport properties but decrease thermal conductivity.[1]

It has been reported that the power factor can be increased by optimizing carrier concentration with doping or quantum-confinement effect.[2−4] Moreover, many studies have been made to minimize the thermal conductivity. For example, the phonon-glass electron-crystal approach as in Skutterudites[5] and clathrates,[6] where loosely bound atoms rattle in cage structures, and the thin-film multilayer approach, where the introduction of interfaces significantly reduces phonon propagation.[1] Indeed, artificial thin-film superlattice structures like Bi_2Te_3/Sb_2Te_3[2] and $PbSe_{0.98}Te_{0.02}/PbTe$[7−9] exhibit very low thermal conductivity, and as a result, *ZT* values were significantly raised. The key feature of these systems is the large number of interfaces introduced by the inherent nanofabrication technique that in turn reduce the lattice thermal conductivity. Interestingly, "nanocomposites" in bulks have been recently identified in the $AgPb_m$-$SbTe_{2+m}$ system where compositional fluctuations at the nanoscopic level seem to play a key role for the previously reported high thermoelectric performance.[10−13] Such nanoscopic inhomogeneities like "intrinsically" embedded nanodispersions increase phonon scattering and hence reduce the thermal conductivity, which enhances the *ZT* value provided that the electrical conductivity is not degraded to a greater degree. Therefore, the "in-situ" nanostructuring becomes a potential

[†] Tsinghua University.
[‡] Toyota Motor Corporation.

(1) Bhandari, C. M.; Rowe, D. M. *CRC Handbook of Thermoelectrics*; CRC Press: Boca Raton, FL, 1995; p 43.
(2) Venkatasubramanian, R.; Siivola, E.; Colpitts, V.; Quinn, B. *Nature* **2001**, *413*, 597.
(3) Hicks, L. D.; Harman, T. C.; Sun, X. S.; Dresselhaus, M. S. *Phys. Rev. B: Condens. Matter Mater. Phys*. **1996**, *53*, R10493.
(4) Dresselhus, M. S.; Chen, G.; Tang, M. Y.; Yang, R.; Lee, H.; Wang, D.; Ren, Z.; Fleurial, J.-P.; Gogna, P. *Adv. Mater*. **2007**, *19*, 1043.
(5) Sales, B. C.; Mandrus, D.; Williams, R. K. *Science* **1996**, *272*, 1325.
(6) Nolas, G. S.; Slack, G. A.; Schujman, S. B. *Semicond. Semimet.* **2001**, *69*, 255.
(7) Harman, T. C.; Taylor, P. J.; Walsh, M. P.; LaForge, B. E. *Science* **2002**, *297*, 2229.
(8) Harman, T. C.; Spears, D. L.; Manfra, M. J. *J. Electron Mater*. **1996**, *25*, 1121.
(9) Beyer, H.; Nurnus, J.; Bottner, H.; Lambrecht, A.; Roch, T.; Bauer, G. *Appl. Phys. Lett.* **2002**, *80*, 1216.
(10) Hsu, K. F.; Loo, S.; Guo, F.; Chen, W.; Dyck, J. S.; Uher, C.; Hogan, T.; Polychroniadis, E. K.; Kanatzidis, M. G. *Science* **2004**, *303*, 818.
(11) Quarez, E.; Hsu, K. F.; Pcionek, R.; Frangis, N.; Polychroniadis, E. K.; Kanatzidis, M. G. *J. Am. Chem. Soc*. **2005**, *127*, 9177.
(12) Wang, H.; Li, J.-F.; Nan, C.-W.; Zhou, M.; Liu, W. S.; Zhang, B.-P.; Kita, T. *Appl. Phys. Lett*. **2006**, *88*, 092104.
(13) Androulakis, J.; Hsu, K. F.; Pcionek, R.; Kong, H.; Uher, C.; D'Angelo, J. J.; Downey, A.; Hogan, T.; Kanatzidis, M. G. *Adv. Mater*. **2006**, *18*, 1170.

approach to enhance the thermoelectric performance of $AgPb_mSbTe_{2+m}$ system bulk materials. Compared with thermoelectric films, thermoelectric bulk materials are conducive to realization of a large temperature difference and industrial applications. $AgPb_mSbTe_{2+m}$ bulk thermoelectric materials are promising for electrical power generation at moderate temperatures ranging from 600 to 900 K.

Our recent work[12] revealed that a powder metallurgy process combining mechanical alloying and spark plasma sintering is suitable for fabricating the $AgPb_mSbTe_{2+m}$ bulk materials, which produces fine-grained materials with enhanced *ZT* values. Compared with the material fabricated by melting and slow cooling reported by Hsu et al.,[10] the $AgPb_mSbTe_{2+m}$ bulks prepared by the combined MA and SPS methods may be very hard to reach an equilibrium state. Therefore, the present work was conducted to mainly study the effect of annealing treatment on the thermoelectric performance and microstructure of Pb-rich $Ag_{0.8}Pb_{m+x}SbTe_{m+2}$ ($m = 18$, $x = 4.5$) compound, which was found to be the optimal composition showing the best thermoelectric properties by our previous study.[14] The thermoelectric performance is greatly enhanced and a large *ZT* value of up to 1.5 is obtained by moderate annealing treatment. The present work revealed the importance of the nanostructuring approach to the development of high-performance thermoelectric materials, which has been realized by a simple annealing method in the $AgPb_mSbTe_{2+m}$ system.

2. Experimental Section

2.1. Synthesis. The commercial elemental powders of Ag (99.9%, powder, 150 μm), Pb (99.9%, powder, 75 μm), Sb (99.9999%, powder, 150 μm), and Te (99.999%, powder, 150 μm) were used as starting materials. The mixtures of these powders were subjected to MA in a planetary ball mill (QM-2L) using a hardened stainless steel vial and balls. The weight ratio of balls to powder was kept at about 20:1, and the mill vial was purged and filled with Ar + 5 atom % H_2 atmosphere to prevent the powders from oxidation during the milling process. The milling was performed at 350 rpm for 4 h, and the MA-derived $Ag_{0.8}Pb_{22.5}SbTe_{20}$ powders were consolidated by SPS at 673 K for 5 min under an axial pressure of 50 MPa. The MA and SPS parameters were confirmed to be suitable for synthesizing the compound from the elemental powders by our previous studies.[12,14] The sintered bulk samples were sealed in vacuum (1×10^{-3} Pa) in glass tubes and annealed for several days (3, 10, and 30 days) at 653 K.

2.2. High-Resolution Transmission Electron Microscopy and X-ray Diffraction. The phase structures of the resultant samples were examined by X-ray diffraction (XRD) using Cu Kα radiation (Rigaku RINT2000). The nanostructure of all the samples was examined using transmission electron microscopy (field emission TEM, JEOL-2011). Specimens used for the investigation were hand polished to about 50−60 μm with sand paper and subsequent diamond paste. Samples were then thinned to electron transparency using a Gatan model 600 CDIF precession ion-milling system at low angle (8−12°). High-resolution transmission electron microscopy images of several different locations inside of the pieces were recorded at 200 kV.

2.3. X-ray Fluorescence Analysis. The chemical compositions of all the samples were analyzed by X-ray fluorescence (XRF) using a XRF-1800 spectrometer equipped with a Rh anode X-ray tube. A reference sample was prepared by forming a powder compact via die pressing using a powder mixture of Ag, Pb, Sb, and Te at a stoichiometric proportion of $Ag_{0.8}Pb_{22.5}SbTe_{20}$.

2.4. Electrical Transport Properties. The carrier concentration and mobility were measured by the bar method using the Hall measurement system (Accent 5500). The Seebeck coefficient and electrical resistivity were measured using the Seebeck Coefficient/Electrical Resistance Measuring System (ZEM-2).

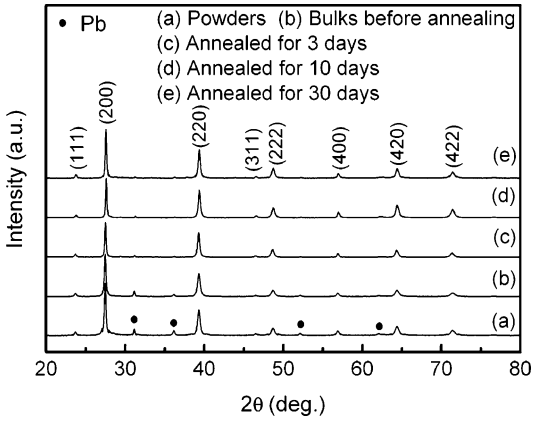

Figure 1. XRD patterns of $Ag_{0.8}Pb_{22.5}SbTe_{20}$ powders (a) and bulks before and after annealing for different times (b−e).

2.5. Thermal Conductivity. The thermal conductivity (κ) was calculated using the equation $\kappa = \lambda C_p d$, where λ is the thermal diffusivity, C_p is the heat capacity, and d is bulk density of the sample. The thermal diffusivity was measured by a laser flash technique (NETZSCH LFA427) in Ar atmosphere in the temperature range 300−700K. The heat capacity was measured using differential scanning calorimety and then confirmed independently at two different test centers. The bulk density was obtained by the Archimedes method.

Lattice thermal conductivities (κ_L) were obtained by subtracting the electrical contribution from the total thermal conductivity using the equation $\kappa_L = \kappa - \kappa_e$. Here, the electrical thermal conductivity is expressed by the Wiedemann Franz Law $\kappa_e = LT/\rho$, where L is the Lorenz number.

3. Results

3.1. Structural Characterization and Hall Measurement. $AgPb_mSbTe_{m+2}$ compounds possess an average NaCl structure ($Fm\bar{3}$ m symmetry). The metals Ag, Pb, and Sb are disordered in the structure on the Na sites, whereas Te occupies the Cl sites. Figure 1 shows the X-ray diffraction patterns of the $Ag_{0.8}Pb_{22.5}SbTe_{20}$ composition at different states: MA-derived powders, bulks before and after annealing for different times. $Ag_{0.8}Pb_{22.5}SbTe_{20}$ compound powders with β-PbTe crystal structure (NaCl structure) were obtained from their elemental powders only by MA. The MA-derived compound powders are of several hundred nanometers, which are much finer compared to the starting elemental powders (several hundred micrometers). No significant difference can be observed between the XRD patterns of MA-derived powders and bulk sample before annealing, which again confirmed that MA is effective to synthesize the $AgPb_mSbTe_{m+2}$ compounds. The phase structure of the obtained bulk sample was kept unchanged after annealing. Although the present compound was the optimized composition showing the best thermoelectric properties for MA and SPS by our previous study,[14] it is worth noting that the Pb content in the $Ag_{0.8}Pb_{22.5}SbTe_{20}$ compound is richer than that of the stoichiometric composition for the $AgPb_mSbTe_{2+m}$ system. As a result, some weak diffraction peaks of Pb were observed in the XRD patterns even for some annealed samples, although the intensity of Pb diffraction peaks decreased after annealing.

The compositions of $Ag_{0.8}Pb_{22.5}SbTe_{20}$ bulks before and after annealing for different times are measured by XRF, and the

(14) Zhou, M.; Li, J.-F.; Wang, H. *Chin. Sci. Bull.* **2007**, *52*, 990−996.

Table 1. Carrier Concentration, Mobility, Electrical Resistivity, and Measured Composition of All Samples at Room Temperature

sample	final composition	carrier concentration [10^{18} cm^{-3}]	carrier mobility [cm^2 V^{-1} s^{-1}]	electrical resistivity [10^{-3} Ohm-cm]
$Ag_{0.8}Pb_{22.5}SbTe_{20}$ before annealing	$Ag_{0.8}Pb_{22.1}SbTe_{20.8}$	6.63	220	4.20
annealed for 3 days	$Ag_{0.7}Pb_{19.7}SbTe_{19.0}$	2.34	513	5.21
annealed for 10 days	$Ag_{0.7}Pb_{19.6}SbTe_{18.1}$	2.96	540	3.90
annealed for 30 days	$Ag_{0.7}Pb_{19}SbTe_{18.9}$	3.26	558	3.43
$AgPb_{18}SbTe_{20}$[a]		0.05	100	

[a]The data for $AgPb_{18}SbTe_{20}$ was from ref 10.

results are summarized in the column of "final compositions" in Table 1. The measured composition is $Ag_{0.8}Pb_{22.1}SbTe_{20.8}$ for the unannealed sample with the nominal composition of $Ag_{0.8}Pb_{22.5}SbTe_{20}$. This result indicates that the starting composition is almost unchanged during MA and SPS. The Pb content in $Ag_{0.8}Pb_{22.5}SbTe_{20}$ bulks decreases apparently with annealing time and then decreases slowly when the annealing time is over 3 days. The XRF results are consistent with the decreased intensity of Pb diffraction peaks shown in Figure 1. The decrease of Pb content is supposed to be due to the volatilization of Pb during the annealing period at high temperature (653 K) in vacuum.

3.2. Thermoelectric Properties. Figure 2a indicates the temperature dependence of the electrical resistivity for $Ag_{0.8}Pb_{22.5}SbTe_{20}$ bulks before and after annealing for different times. The electrical resistivity of the unannealed sample is about 7 $\times$ 10^{-3} Ohm-cm at room temperature and then decreases with temperature, indicative of semiconducting transport behavior. The electrical resistivity value of the unannealed sample with a nominal composition of $Ag_{0.8}Pb_{22.5}SbTe_{20}$ materials is much lower than that of the $AgPb_{18}SbTe_{20}$ compound reported by K. F. Hsu[10] and Y. G. Yan et al.[15] The reason for this difference may be mainly related to the higher electron concentration caused by the free Pb in our samples, as shown in Table 1. The electrical resistivity increases a little when annealed for 3 days and then decreases with annealing time. For example, the electrical resistivity decreases to 4 $\times$ 10^{-3} Ohm-cm for the sample annealed for 30 days at room temperature. In the measured temperature range, the electrical resistivity of all the annealed samples increases with temperature and then decreases when the temperature is over 400 K, showing a semimetallic to semiconducting transforming behavior at 400 K.

Figure 2b shows the temperature dependence of Seebeck coefficient for $Ag_{0.8}Pb_{22.5}SbTe_{20}$ bulks before and after annealing for different times. The negative Seebeck coefficient values are indicative of n-type electrical transport properties. The absolute value of Seebeck coefficient $|\alpha|$ increases with annealing time and reaches a maximum value of 287 μV K^{-1} at 450 K when annealing time reaches to 3 days but decreases gradually when the annealing time is over 3 days. This change is consistent with that of electrical resistivity. For the annealing experiments, the sintered samples were encapsulated and heated in sealed glass tubes. Some free Pb would volatilize during the annealing treatment, as confirmed by XRD and XRF results. The vapor pressure of Pb inside the glass tubes gradually reached its saturated value, and volatilization of free Pb would become more and more difficult as the annealing time was further prolonged.

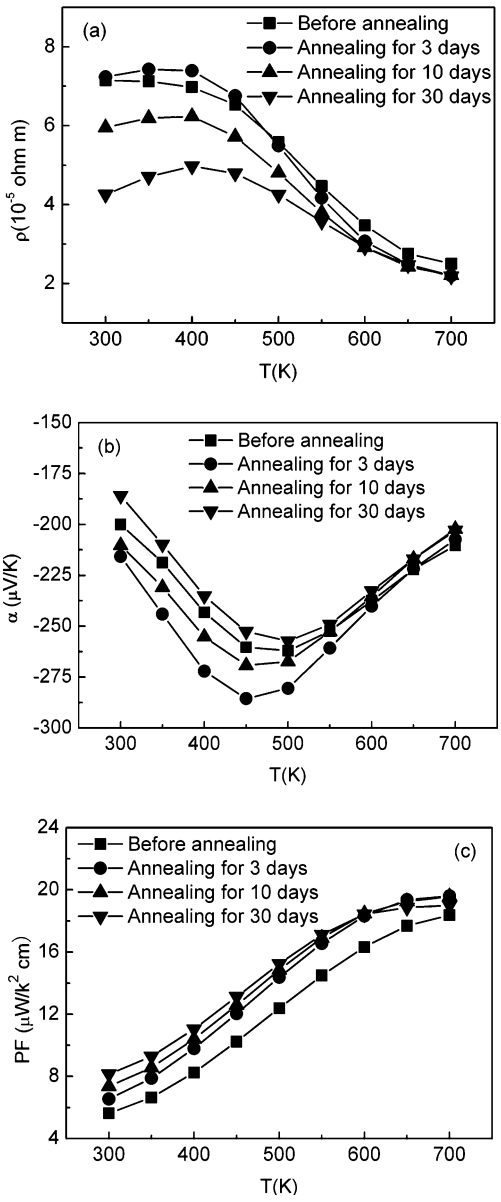

Figure 2. Temperature dependence of (a) electrical resistivity, (b) Seebeck coefficient, and (c) power factor value for $Ag_{0.8}Pb_{22.5}SbTe_{20}$ bulks before and after annealing for different times.

On the other hand, the distortion of the lattice and defects introduced by the mechanical alloying process was reduced and even vanished with increasing annealing time. Therefore, the electron concentration greatly decreased due to the volatilization of free Pb at the starting period of the annealing treatment. The electron concentration of 6.63 $\times$ 10^{18} cm^{-3} for the unannealed sample decreased to 2.34 $\times$ 10^{18} cm^{-3} for the sample annealed for 3 days. However, as the annealing time was further increased, the electron concentration changed little because the volatilization of free Pb became very difficult. At the same time, the carrier mobility increased because carrier scattering weakened as a result of the reduced lattice distortion and defects due to annealing treatment, as shown in Table 1. Thus, we believe that the increase of electrical resistivity and $|\alpha|$ with annealing time is mainly caused by the decrease of electron concentration resulting from volatilization of free Pb at the starting period of the annealing treatment, although the carrier mobility increased. When the annealing time is over 3 days,

(15) Yan, Y. G.; Tang, X. F.; Liu, H. J.; Yin, L. L.; Zhang, Q. J. *Acta Phys. Sin.* **2007**, *56*, 3473 (in Chinese).

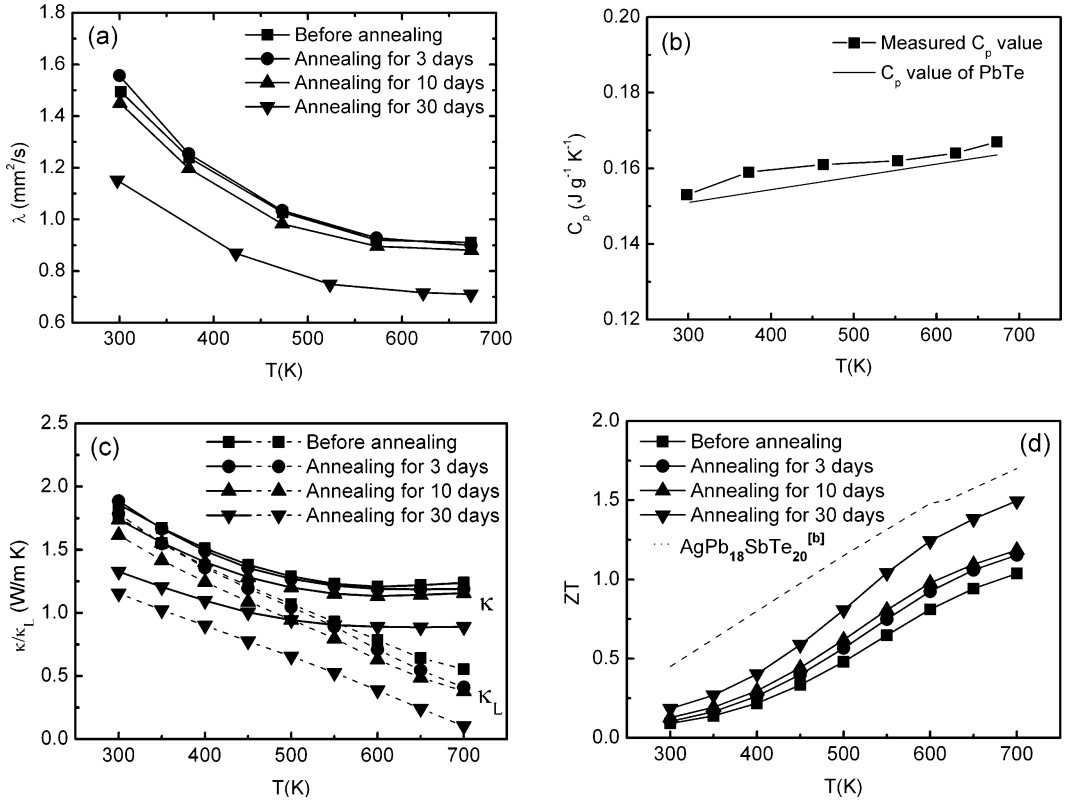

Figure 3. Temperature dependence of (a) thermal diffusivity, (b) measured heat capacity, (c) thermal conductivity, and (d) *ZT* value for $Ag_{0.8}Pb_{22.5}SbTe_{20}$ bulks before and after annealing for different times. (b) The data for $AgPb_{18}SbTe_{20}$ was from ref 10.

the decrease of electrical resistivity and |α| with annealing time is mainly caused by the increased carrier mobility. The absolute value of the Seebeck coefficient for all samples increased and showed a peak at about 400−500 K and then decreased with increasing temperature. Below 400−500 K, |α| increased with increasing temperature, indicating that the conduction could be dominated by extrinsic charge carriers excited from the impurity state. Above 400−500 K, |α| decreased with increasing temperature, which was considered to be due to excitation of electron−hole pairs across the energy gap, because their opposing contributions to the Seebeck coefficient from the two carriers reduced the observed |α|. With the above values of electrical resistivity and Seebeck coefficient, we calculated the power factor values of all the samples, as shown in Figure 2c. The power factor values showed an increasing trend with increasing annealing time. A large power factor (>19 μW K^{-2} cm^{-1}) has been obtained for the annealed samples in a wide temperature range of 600−700 K.

The thermal conductivity (κ) is calculated from the thermal diffusivity (λ), the heat capacity (C_p), and the density (d), $\kappa = \lambda C_p d$. The thermal diffusivity was measured by a laser flash technique, and the results are shown in Figure 3a. The thermal diffusivity was reduced with annealing time; in particular, the thermal diffusivity of the sample annealed for 30 days greatly decreased. The minimum thermal diffusivity is 0.7 mm^2/s at 673 K. The measured density values of the unannealed sample and the samples annealed for 3, 10, and 30 days are 8.08, 7.92, 7.82, and 7.56 g cm^{-3}, respectively. In this paper we evaluated the C_p value of all the samples by the DSC method for over three times in different apparatus. The measured C_p values are consistent with each other for the samples before and after annealing, which may be attributed to little change of composition and crystal structure. Figure 3b shows the measured representative C_p values. The C_p value increased a little with temperature, and the minimum C_p value is 0.153 J g^{-1} K^{-1} at room temperature. The measured C_p values are larger than those of PbTe during the measured temperature range, as shown in Figure 3b. We calculated the thermal conductivities of all the samples with the above measured thermal diffusivity, density at room temperature, and heat capacity and show the results in Figure 3c. The thermal conductivity of the unannealed sample is 1.86 W m^{-1} K^{-1} at room temperature. This value is a little higher than our previously reported result because the measured C_p values are larger than those of PbTe compound used in previous papers.[12,14] The thermal conductivity of the sample annealed for 30 days significantly decreases, and a low thermal conductivity of 0.89 W m^{-1} K^{-1} is obtained at the temperature range of 550−700 K. This value is just two-thirds of the unannealed sample at the same temperature range. As we know, thermal conductivity can be expressed by the sum of lattice component (κ_l) and electronic component (κ_e) as $\kappa = \kappa_l + \kappa_e$. κ_e can be estimated from Wiedemann−Franz's law as $\kappa_e = LT/\rho$, where L is the Lorenz number (2.45×10^{-8} V^2 K^{-2} for free electrons), and $\kappa_l = \kappa - \kappa_e$. The κ_e values increase with annealing time because of the decreased electrical resistivity. Thus, the decrease of thermal conductivity can be mainly attributed to the significant reduction of lattice thermal conductivity caused by the enhanced nanopoint defects scattering with annealing time. From Figure 3c we can also see that the thermal conductivity and lattice thermal conductivity decrease with increasing annealing time, which is due to the increased phonon−phonon scattering at high temperature.

According to the measured electrical resistivity, Seebeck coefficient, and thermal conductivity, we calculated *ZT* values

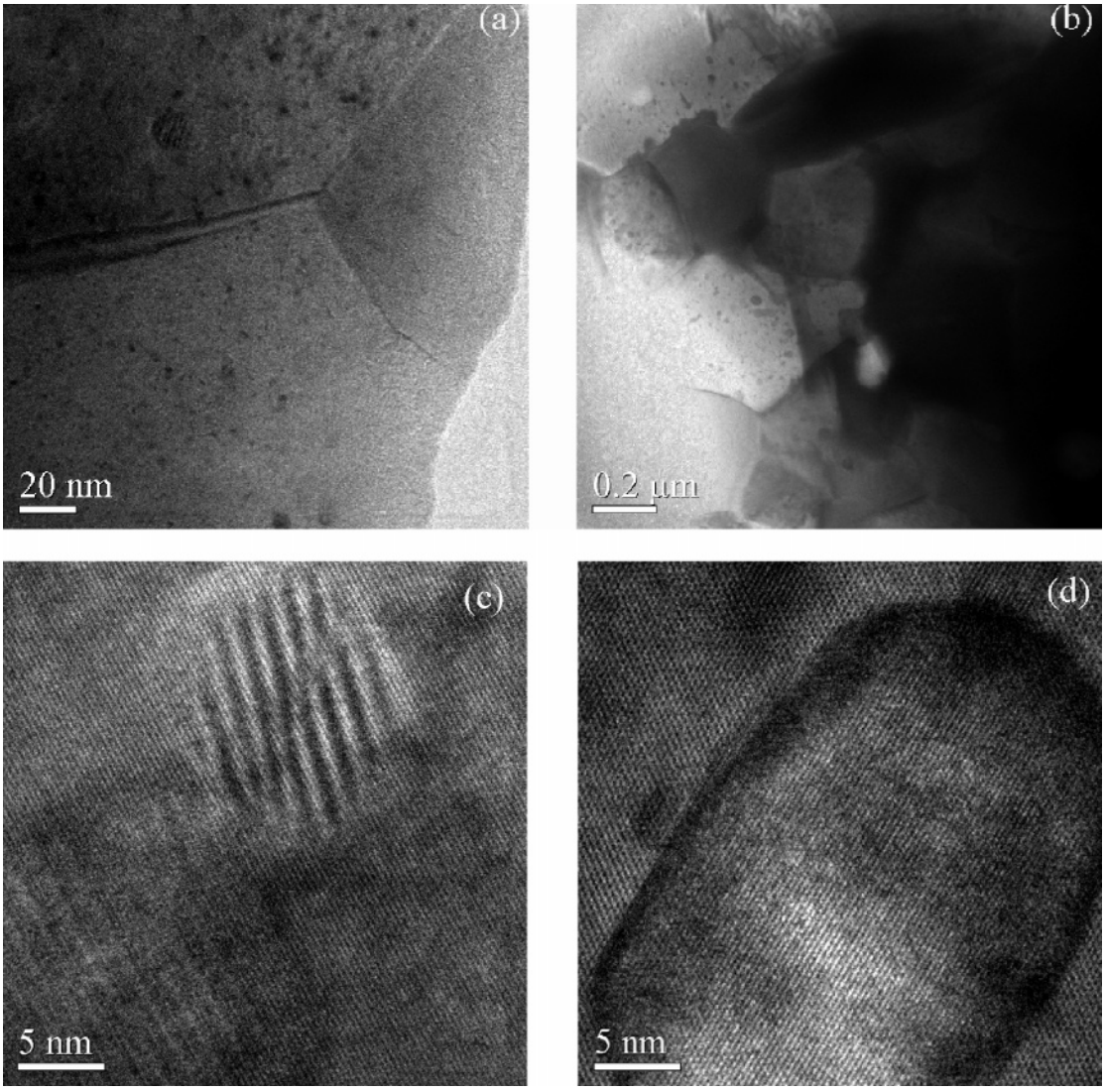

Figure 4. Low-magnification TEM images of (a) unannealed sample and (b) the sample annealed for 30 days. HRTEM images of (c) unannealed sample and (d) the sample annealed for 30 days.

using the expression, $ZT = \alpha^2 T/\rho\kappa$. The temperature dependence of *ZT* is shown in Figure 3d. The maximum *ZT* value of the unannealed sample is 1.05 at 700 K, and it was enhanced with annealing time. A maximum *ZT* value of 1.5 has been obtained for the sample annealed for 30 days at 700 K. This value is very close to the maximum *ZT* value of 1.7 (the dashed line shown in Figure 3d) at 700 K for the $AgPb_{18}SbTe_{20}$ alloy reported by K. F. Hsu et al.,[10] which was fabricated by a special melting and slow cooling method, which may be more complicated than the present powder-based fabrication process combining MA and SPS. It is worth noting that the decrease of both the electrical resistivity and the thermal conductivity plays a key role in enhancing the figure of merit for the annealed samples because of the increased nanoscopic regions inside of crystal grains. As we know, it is very hard to simultaneously reduce ρ and κ for most thermoelectric materials.

4. Discussion

We mentioned that the distortion of lattice and defects were reduced and even vanished with increasing annealing time, which may weaken the scattering effects of carriers and phonons and increase thermal conductivity. In fact, the thermal conductivity of the annealed samples did not increase but decreased with annealing time. Why? We think there must be some other scattering mechanisms besides the above scattering effect. As we know, the $Ag_{0.8}Pb_{22.5}SbTe_{20}$ compound possesses an average NaCl structure ($Fm\bar{3}m$ symmetry). Some Pb^{2+} sublattices were isoelectronically substituted by Ag^+ and Sb^{3+}. The formula is charge balanced because the average charges on the metal ions and the chalcogen ions are 2^+ and 2^-, respectively.[10] However, how are the Ag^+ and Sb^{3+} ions distributed in the structure, i.e., homogeneously or not homogeneously? If Ag^+ and Sb^{3+} are homogeneously dispersed in the $Fm\bar{3}m$ lattice, it would require the complete separation of the Ag^+ and Sb^{3+} pair over a long distance, resulting in charge imbalances in the vicinity of these atoms. Thus, Ag^+ and Sb^{3+} ions are inclined to form Ag^+-Sb^{3+} pairs to keep charge balance in the $Ag_{0.8}Pb_{22.5}SbTe_{20}$ compound with increasing annealing time.[10] In fact, we indeed observed a lot of nanoscopic black regions embedded in the PbTe-rich matrix in the transmission electron microscopy (TEM) images for all the samples before and after annealing treatment. TEM images of the sample before and after annealing for 30 days

are shown in Figure 4a and b. Clearly, the number and size of these nanoscopic regions increase with annealing time. These nanoscopic regions can only be probed through a detailed examination of the structure at the atomic scale. Thus, we performed high-resolution transmission electron microscopy (HRTEM) images on all samples. The HRTEM images of the unannealed sample revealed the existence of nanoscale features. As shown in Figure 4c, we can see a certain amount of localized wavy pattern with a size of about 5−10 nm inside of all the crystal grains. These nanostructures are coherent with their surrounding crystal matrix. They should be related to compositional fluctuations between Ag, Sb, and Pb based on the above charge-balance theory. That is, Ag/Sb-rich regions are formed and embedded in the surrounding matrix endotaxially without disturbing the electronic flow. The HRTEM images of annealed samples, for example, the sample annealed for 30 days, displayed larger nanoscopic regions with a size of 10−50 nm, as shown in Figure 4d. It was also found that the numbers of this kind of nanoscopic regions greatly increased compared to the unannealed sample. The increased nanoscopic regions and surrounding nanointerfaces are thought to strongly scatter phonons, especially the intermediate frequency heat-carrying phonons.[16] As a result, the thermal conductivity of the annealed samples dropped compared to the unannealed sample. Some similar HRTEM results in the melted $Ag_nPb_mSb_nTe_{m+2n}$ bulks were also reported by Hsu et al.[10]

(16) Li, D.; Huxtable, S. T.; Abramson, A. R.; Majumdar, A. *J. Heat Transfer*. **2005**, *127*, 108.

5. Conclusions

The nanostructured $Ag_{0.8}Pb_{22.5}SbTe_{20}$ compounds have been fabricated by mechanical alloying and spark plasma-sintering method. The electrical transport properties and thermal conductivity, especially the heat capacity, were carefully examined in a temperature range of 300−700 K. As a potential thermoelectric material, $Ag_{0.8}Pb_{22.5}SbTe_{20}$ has a high power factor of nearly 18 μW K^{-2} cm^{-1} and low thermal conductivity of 1.2 W m^{-1} K^{-1} at high temperature. The thermoelectric properties of these compounds have been enhanced by annealing treatment. The thermal conductivity is greatly reduced with annealing time, and a minimum thermal conductivity value of 0.89 W m^{-1} K^{-1} is obtained at 700 K for the sample annealed for 30 days. It is very interesting that the power factor does not decrease but increases with annealing time over the measured temperature range. As a result, a large *ZT* value of 1.5 has been obtained for the sample annealed for 30 days at 700 K. The HRTEM investigation reveals an increased amount of nanoscopic inhomogeneities inside of grains by annealing treatment. Such nanoscopic inhomogeneities are considered to result mainly in the enhanced phonon scattering and the great reduction of thermal conductivity.

Acknowledgment. The authors acknowledge financial support from the National Basic Research Program of China (Grant No. 2007CB607505), Tsinghua-Toyota collaborative research project (No. 0307J36), National Natural Science Foundation of China (No. 50621201), Natural Science Foundation of Beijing (Grant No.2072009), and China Postdoctoral Science Foundation (Grant No.20060390042).

JA7110652